3D-microfabrication by two-photon polymerization of an integrated sacrificial stencil mask

Puce, Salvatore; Sciurti, Elisa; Rizzi, Francesco; Spagnolo, Barbara; Qualtieri, Antonio; De Vittorio, Massimo; Staufer, Urs

DOI
10.1016/j.mne.2019.01.004

Publication date
2019

Document Version
Final published version

Published in
Micro and Nano Engineering

Micro and Nano Engineering 2 (2019) 70–75

Contents lists available at ScienceDirect

Micro and Nano Engineering

journal homepage: www.journals.elsevier.com/micro-and-nano-engineering

3D-microfabrication by two-photon polymerization of an integrated sacrificial stencil mask

Salvatore Puce[a,b,*], Elisa Sciurti[a,b], Francesco Rizzi[a,*], Barbara Spagnolo[a], Antonio Qualtieri[a], Massimo De Vittorio[a,b], Urs Staufer[a,c]

[a] Center for Bio-Molecular Nanotechnologies@Unile, Istituto Italiano di Tecnologia, Via Eugenio Barsanti 14, 73010 Arnesano, LE, Italy
[b] Dipartimento di Ingegneria dell'Innovazione, Università del Salento, Complesso Ecotekne, edificio "Corpo O, Via per Monteroni, 73100, Lecce, Italy
[c] Delft University of Technology, Delft, 2628, CD, The Netherlands

ARTICLE INFO

Keywords:
Stencil lithography
Stencil mask
3D metallization
Two-photon polymerization lithography

ABSTRACT

This work aims at developing a new and unconventional Sacrificial Stencil Mask (SSM) technology by exploiting Two-Photon Polymerization (2PP) in an IP-L/SU-8 double layer resist system. The process consists of the sequential deposition of two different resists, such as SU-8 and IPL, onto the same glass substrate, followed by 2PP lithography and distinct development processes. The 2PP writing process was used to polymerize structures inside the top and bottom resist layers to form, in one single exposure process, both SSM and a permanent polymeric structure, in our case a plain pedestal. The top IPL resist was developed using Isopropyl Alcohol (IPA), which does not affect either exposed or un-exposed SU-8 regions. In this way, structures written into the bottom layer remained latent, while exposed areas of the top IPL resist, including the stencil mask, were developed. The realization of 3D stencil masks, designed to be anchored inside the un-exposed bottom layer, was combined with metal evaporation to demonstrate the deposition of a plain metal line through the stencil mask. The final development of the bottom layer led to the lift off of the sacrificial stencil mask, uncovering the underlying, permanent polymer-metal structure. The combination of sacrificial polymer structures with permanent ones opens new possibilities in 3D MEMS design, enabling the integration of distributed electronic transducers in flexible polymeric structures.

1. Introduction

The use of stencils is one of the oldest technologies in human history, for which evidence is found from over 35,000 years ago [1]. Stencil lithography (SL) is based on the principle of shadow masking a flux of atoms, molecules or particles to locally modify a substrate surface by different methods such as deposition, etching or ion implantation, which are well established in 2D microfabrication [2–8]. There are different implementations of stencils which are made of materials such as polymers or metals which can withstand the processing conditions. The spacing between substrate and stencil is critical in terms of pattern definition. Some implementations employ therefore a rigid but temporary connection with the substrate [9], which has a close similarity with the so-called lift-off technique [10,11]. These stencils are normally sacrificed after use. On the other hand, stencils, which are entirely separated from the substrate and positioned by means of a manipulator, can be reused many times. This allows cost-effective pattern replication with various materials onto different substrates. These stencils can also be moved with respect to the substrate during deposition in order to obtain a dynamic lithography. The potential of SL for a broad range of materials, processes and applications has been demonstrated by numerous reports [12]. Micro-Stencils face important challenges, namely membrane stability, clogging and blurring [13]. Membrane instability occurs because the stencil membrane is not in intimate contact with the substrate, since stress, curvature, or topography prevent a complete contact between the stencil and the substrate. In some cases this lack of contact can be beneficial to preserve a fragile substrate, but it can also compromise the definition of the pattern. The accumulation of the material on the membrane and inside the apertures produces a significant reduction in the size of the opening mostly if the stencil aperture size is similar or smaller than the thickness of the deposited material. This effect can be used to create even smaller or conical patterns, but it ultimately affects the reproducibility of the deposited patterns and limits the reutilization of the stencils. Finally, the size of the blurring can be in the same range, or even bigger, than the aperture size itself. In fact, due to the divergence of material flux, and the gap

* Corresponding author at: Center for Bio-Molecular Nanotechnologies@Unile, Istituto Italiano di Tecnologia, Via Eugenio Barsanti 14, 73010 Arnesano, LE, Italy.
E-mail addresses: salvatore.puce@iit.it (S. Puce), francesco.rizzi@iit.it (F. Rizzi).

https://doi.org/10.1016/j.mne.2019.01.004
Received 26 October 2018; Received in revised form 11 January 2019; Accepted 26 January 2019

between the stencil and the substrate, the stencil apertures are inherently smaller than the structures deposited through stencils.

Typical applications of Two-Photon Lithography (2PL) are in the fabrication of mechanical [14] or optical [15] meta-materials, small micro-mechanical devices [16], or 3D micro-experimental set-ups for investigating cells mechanics and biochemical and biophysical properties [17,18]. The primary material of structures fabricated by 2PL is the photo-sensitive polymer itself. More complex structures using different polymers can be fabricated if a second 2PL is aligned to a previously written structure [19]. The polymer structures can also be modified to generate metallic [20,21] or ceramic structures [21]. Alternatively, post-processing steps such as atomic layer deposition [22], electroplating [23] or electro-less plating [24] can be used to coat the polymer with a thin film or to fill the space in between the polymeric features thus generating an inverted replica. Each of these methods has in common that the entire structure is made of the same material or is uniformly coated with the same material. For some applications, though, it would be advantageous to integrate conductive metal lines or sensing elements on specific locations of the polymeric structure only.

Our work introduces a novel approach to generate such mixed-material 3D microstructure by combining stencil mask patterning with Two-Photon Polymerization (2PP) through a double layer resist technology. The 3D Sacrificial Stencil Masks (SSM) is combined with metal evaporation, which allows incorporating electronic devices on polymeric structures thus producing unconventional 3D device architectures. Using a double layer resist enables writing the polymeric scaffold and a SSM in one single exposure process, eliminating tedious alignment procedures. The gap and the alignment between the SSM and the scaffold can be fine-tuned to the resolution of 2PL. Changing the evaporation angles between two consecutive deposition runs allows to generate material junctions e.g. for fabricating a mesh of thermocouples. After the evaporation processes, the SSM is removed.

2. Methods

Our approach is based on 2PL and uses two different layers of negative resists, each of them with different development chemistry and process. Thanks to this double layer, it is possible to sequentially develop the structures layer by layer with intermediate processing steps between the developments. The concept foresees that one resist forms a base-layer in which we expose areas for placing permanent structures and leave areas unexposed for anchoring temporary or sacrificial structures. The SSM and the permanent polymeric structure, in our demonstrator-case a plain pedestal, are exposed in the top layer.

The base or bottom-layer, in our case SU-8, is spin-coated on the glass-substrate normally used for 2PL. Then, a droplet of the top resist, here IP-L (IP-L is a negative resist, proprietary chemical formulation of company Nanoscribe), is placed on top of the spin-coated layer Fig. 1(i).

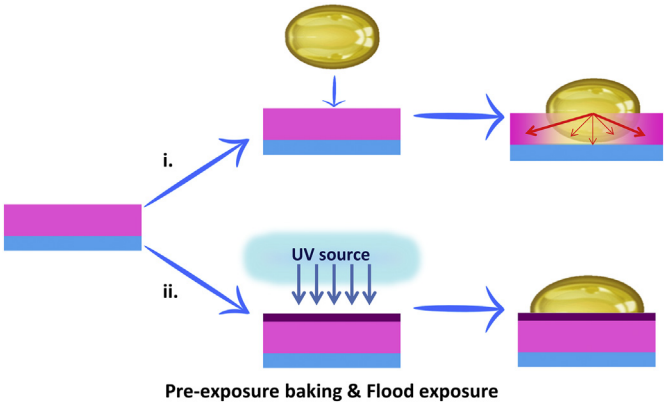

Fig. 2. Double layer resists deposition
i. Diffusion of the top resist into the bottom one
ii. Flood-exposure prevents the diffusion of the two resists

This top layer can be spin-coated or, as normally done in 2PL, left as is. After that, the 2PP writing process is used to polymerize the structures inside the resists Fig. 1(ii). In one single lithographic process both structures, the SSM and the permanent pedestal, are written. It is important to note that the pedestal is written in both resists, allowing the metal to be deposited on its top surface, while the SSM is only anchored in the unexposed bottom layer. The top resist is developed using a solvent (IPA) that does not dissolve either exposed or un-exposed regions of the bottom resist Fig. 1(iii). Therefore, the structures written into the bottom layer remain latent, while exposed areas of the top one are developed. After the metallisation step Fig. 1(iv), also the bottom section is developed, which lifts off the SSM and exposes the permanent metal-polymer structure Fig. 1(v).

2.1. Double layer resists deposition

While preparing the double layer resist system using SU-8 and IP-L, we observed that the IP-L diffuses into the underlying SU-8. This causes changes in optical and chemical characteristics of the bottom layer (see Fig. 2). We investigated this phenomenon by means of fluorescence microscopy in which IP-L can be identified due to its autofluorescence, and found that a short flood-exposure of the SU-8 prior to depositing IP-L could be used to prevent this disturbing effect.

In detail we use spin-coated SU-82025 and droplet-dispensed IP-L 780. In order to visualize the permeation behaviour of the photoresist, a single reference layer of 3 µm SU-82002 mixed with rhodamine b, a red fluorescent dye (designated SU-8/Rho), is spin coated on the glass substrate and baked. Then, 15 µm SU-82025 (not fluorescent) bottom layer is spin coated and again baked, and finally IP-L (green

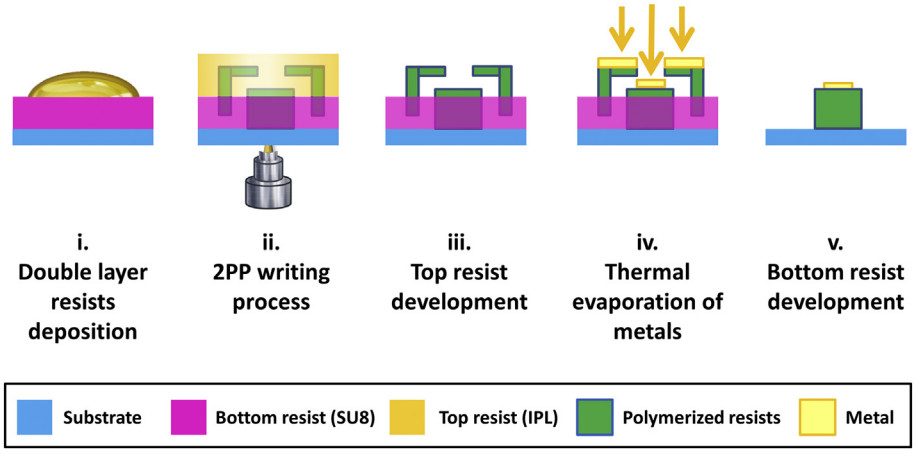

Fig. 1. Fabrication process flow.
(i) Spin coating of bottom resist and drop casting of the top resist.(ii) 2PP writing process of Sacrificial Stencil Mask and pedestal in one single step. Exclusive development of the top layer (iii) followed by the metal evaporation step (iv). After the bottom resist development (v), the structure is fabricated.

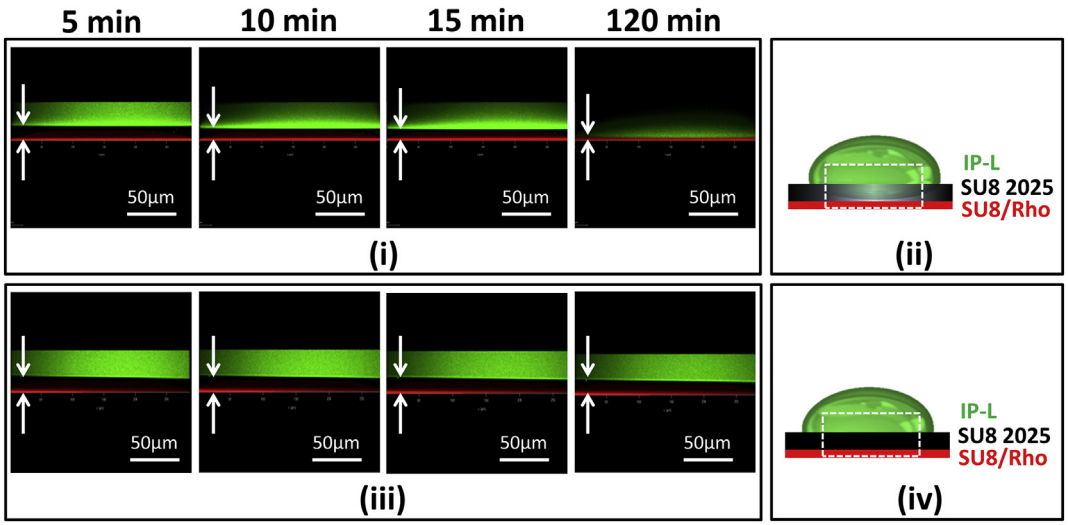

Fig. 3. Confocal z-stack images and schematic illustrations of IP-L drop diffusion into SU-8 layer at different time intervals.
Untreated sample(i) (ii): IP-L drop diffusion into SU-8. Flood-treated sample (iii) (iv): absence of IP-L diffusion into SU-8 underlying layer.

autofluorescence) is dropped on the surface of it (Fig. 3(iii) and (iv)). Imaging is done in a confocal laser scanning microscope (Leica TCS SP8) using a 40× oil immersion objective (HC PL APO CS2, 40×/1.30 OIL) Excitation is achieved through a 405 nm laser for IP-L 780 photoresist and a 540 nm laser for SU-8/Rho. Corresponding fluorescence emissions are in the range 450–550 nm (IP-L 780) and 565–700 nm (rhodamine b), respectively. Confocal z-stack images (z step size of 0.5 µm) collected at different time intervals are shown in Fig. 3. The untreated sample shows an advancing diffusion depth of IP-L (green layer in Fig. 3(i)) into SU-8 bottom layer (not fluorescent layer in Fig. 3). After 2 h (time 3, in Fig. 3(i)) SU-8 bottom layer is completely penetrated.

For the second sample shown in Fig. 3(iii), a flood-exposure treatment (365 nm, 6.5mJ/cm^2, 8 s) is applied prior to depositing the IP-L drop. In this case, no diffusion of IP-L into SU-8 is observed. Fig. 4 illustrates the different interaction between the two resists in both conditions at the edges of the drop.

Based on the confocal images, the depth of penetration in the untreated sample in time (0, 5, 10, 15, 20, 25, 40, 120 min) and at room temperature is measured by Image J. From Fick's second law, describing the diffusion behaviour of IP-L into visco-poro-elastic SU-8 [25], the following equation

$$L_D = \sqrt{4Dt} \quad (1)$$

with L_D,D and t respectively the diffusion length, the diffusion coefficient and the time, allows to calculate the diffusion coefficient.

The depth of penetration of IP-L into the untreated SU-8 is indeed found to follow the square root law as function of the time (Fig. 5), and by fitting the data the diffusion coefficient is found to be D = 8,3*10^{-3} µm^2 / s.

2.2. Design of the stencil mask

For the current demonstrator experiments, the stencil mask is a plain slit, placed on top of a 50 µm high cylindrical tower, golden colored in Fig. 6, while the scaffold is a cuboid pedestal self-aligned with the slit in Fig. 6, being the entire geometry written in the same 2PP process. The slits at the foot of the tower are added to facilitate the development of the structure.

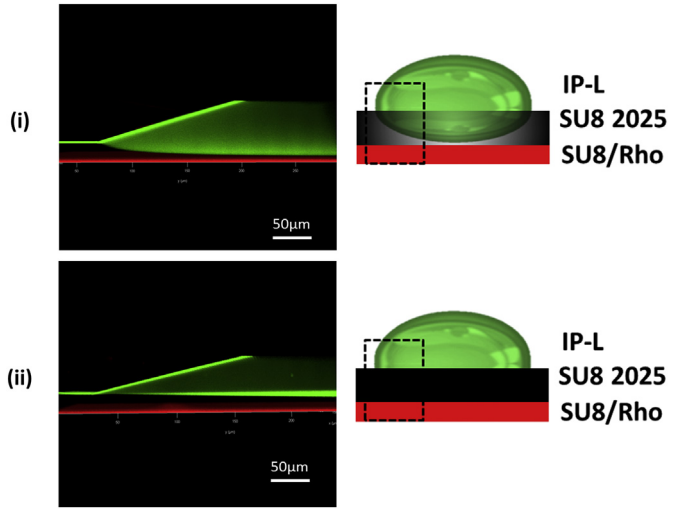

Fig. 4. IP-L drop diffusion into SU-8 layer at the edge of the drop.
Confocal z-stack images and schematic illustrations of untreated sample(i) and flood-treated sample (ii) at the edge of the drop: diffusion profiles of IP-L 780 into SU-8 bottom layer.

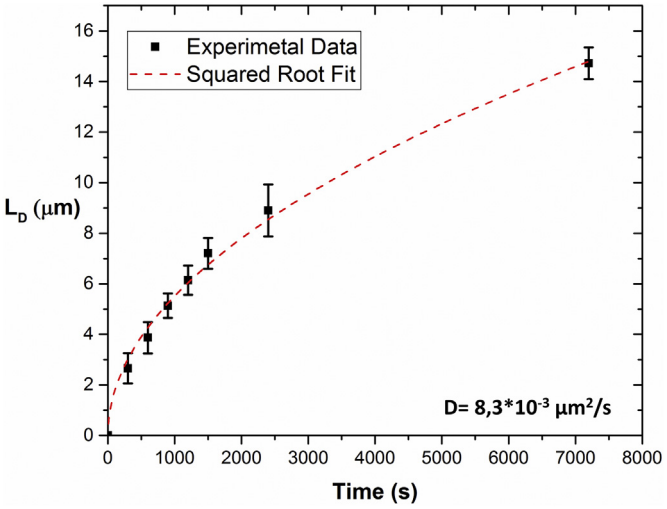

Fig. 5. IP-L diffusion depth profile as function of time fitted with a square root function.

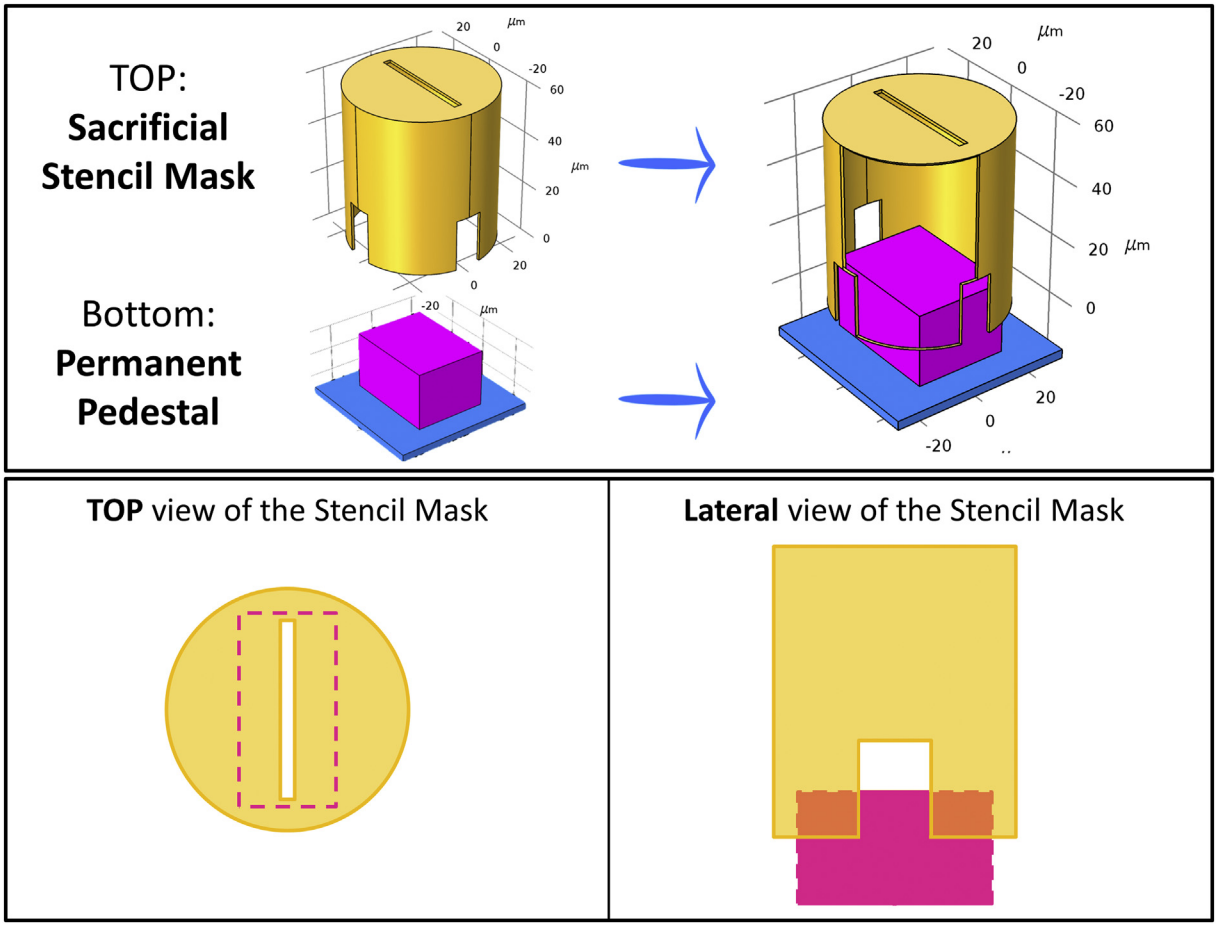

Fig. 6. Design of the Substrate and the Sacrificial Stencil Mask.
This mask allow depositing a rectangular metallic stripe on the top surface of the pedestal. The location of this deposit can be shifted by tilting the axis of the tower with respect to the line-of-sight with the evaporation source. This can be achieved e.g. by means of a wedged shim onto which the substrate is placed during evaporation.

3. Experimental results and discussion

Once the diffusion barrier technique developed, the SSM processing is tested as follows. We first spin coat a 20 µm thick layer of SU-8 for defining the anchoring zones for the permanent and temporal structures respectively. After pre-exposure baking and short UV flashing for conditioning the SU-8 top surface, we deposit a droplet of IPL resist. In one single 2PP lithography step, we first expose the anchoring areas in the SU-8 layer, and then the 3D structures on top of them, while the stencil mask is exposed in the volume on top of unexposed SU-8 areas. After the development of the IPL in IPA (Fig. 7), Cr was evaporated.

Fig. 8 shows the SEM images of the 3D structure with SSM after the metallization with Cr. In Fig. 8(i) the top surface of the fabricated stencil mask is bent due to the residual stress and to the insufficient thickness of the polymerized layer. It is possible to overcome this issue by changing the mechanical structure of the top surface and a re-parameterizing the writing process in terms of exposure time and laser power in order to obtain a stiffer polymerized layer. In Fig. 8(ii) it is

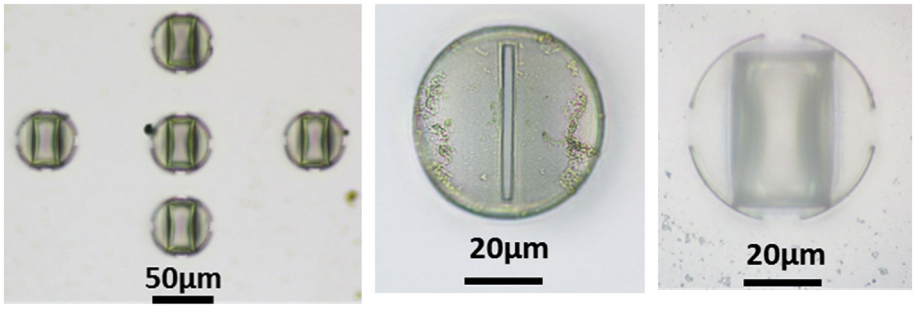

Fig. 7. Optical images of the structures realized by 2PP after development of the top resist in IPA but prior to metallization
i. the SU-8 pedestals and anchoring areas
ii. zoom in, focused on the top part of the SSM, showing the slit
iii. same structure as 7ii, however focused at the level of the pedestal

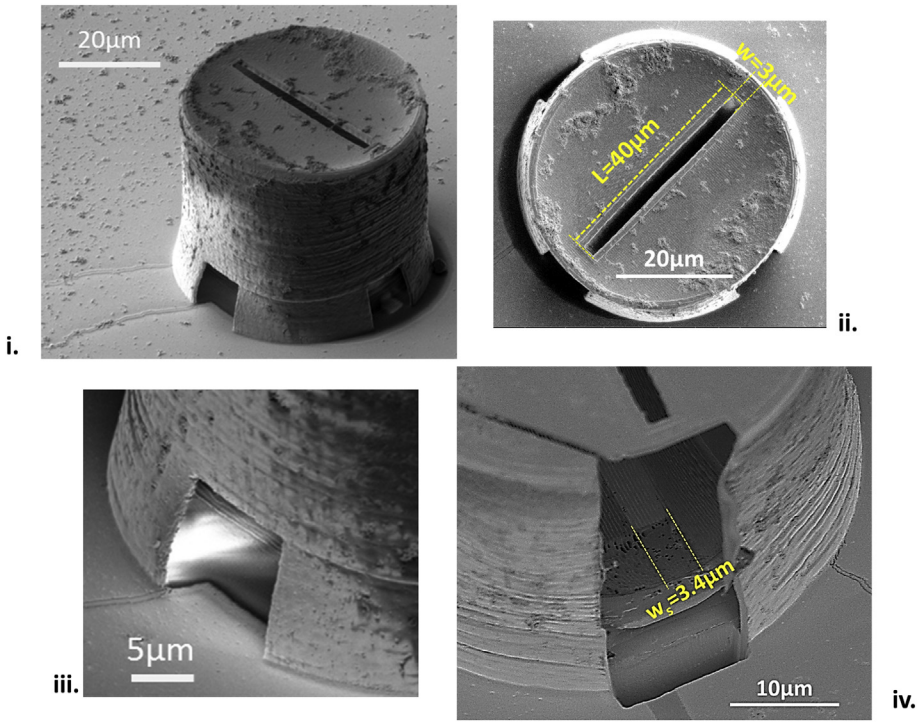

Fig. 8. SEM image of the 3D structure with Sacrificial Stencil Mask after the metallization with Cr
i. The realized stencil mask
ii. The slit length was 40 µm and the width 3 µm.
iii. Section of the stencil mask
iv. Stencil mask opened by Focused Ion Beam milling. It is possible to see the metal structure (yellow dashed line) which has a width of w_s = 3.4 µm.

possible to observe the yellow dashed line that reproduces the geometric dimensioning of the slit while Fig. 8(iv) is the SEM images of the stencil mask opened by Focused Ion Beam milling (FEI dual-beam HeliosNanoLab600i, Ga-ions, beam voltage 1.00 kV, beam current, 0.34 nA) and it is possible to observe the yellow dashed line that is the metal deposited structure width of w_s = 3.4 µm.

After the metallisation step, the stencil mask is lift-off by developing the unexposed SU-8 in the standard SU-8 developer (1-methoxy-2-propyl acetate, bought from MicroChem), which does not affect the polymerized IPL but simply lifts off all those structures that have been written on top of un-exposed SU-8. The downside of the flood treatment is the 'skin' of polymerized SU-8 that is formed at the interface, and which makes lifting off the stencil mask difficult and required ultrasonic excitation during the development. Fig. 9 shows the metal line deposited on the rectangular permanent polymeric pedestal after having lift-off the stencil mask. The arc structures around the pedestal are residues of the sacrificial mask, which as indicated before were difficult to entirely remove.

A zoom-in of Fig. 9 is shown in the optical image in Fig. 10(i) depicting the metal-shadow deposited on the pedestal. The location of this deposit was shifted by tilting the axis of the tower relative to the line-of-sight with the evaporation source. The red dashed line indicates the normal projection of the slit. A shift of 3.1 µm (center to center) was

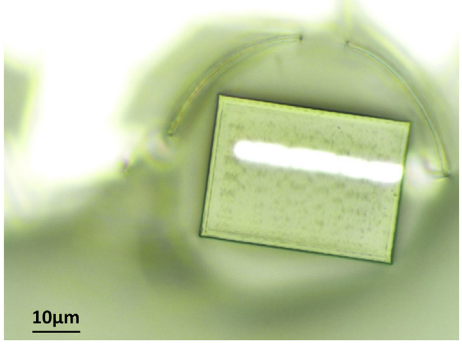

Fig. 9. Optical image of the polymeric pedestal after lift-off of the stencil mask.

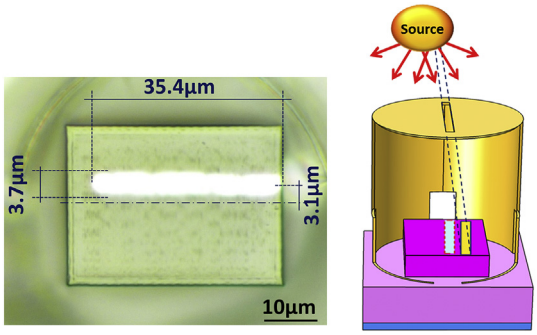

Fig. 10. Optical image of the metal structure after lift-off of the stencil mask.

measured due to the parallaxes between the position of the sample and the Cr source Fig. 10(ii). The analyses of the metal shadow shows a measured width of 3.7 µm instead of the nominal width of 3 µm. This is due to the divergence of the evaporation source, which we assess to be 0.03 rad.

(i) Detail of the developed permanent pedestal with the metal deposited structure; it has a length of 35.4 µm, a width of 3.7 µm. It is shifted by 3.1 µm relative to the normal projection of the stencil (ii)

4. Discussion and conclusions

A new method for fabricating multi-material 3D microstructures has been successfully demonstrated. It is based on Two-Photon Lithography and uses two different negative resists for fabricating an integrated sacrificial stencil masks for local metallization. An essential step is to polymerize a thin interfacial layer between the two resist in order to prevent diffusion of them. The downside of this step is the 'skin' that is formed at the interface, and which can make lifting off the stencil mask difficult. In fact, the thinner the exposed thickness, the easier it is to perform the lift off as this film will need to physically rupture during that process. To this end, we successfully applied ultrasonic excitation, however further improvement is needed.

A bromograph (Edison-delta srl) is used to perform the UV flood exposure by an unfiltered Hg-lamp (6,3 mW/cm^2), usually employed for fabricating electronic boards. The exposure is manually started and stopped, which limits the accuracy and precision. Using a mask aligner would allow a better control of the exposure dose, which would lower the degree of polymerization in the film, and hence, reduce its mechanical strength. Wavelengths beyond ~300 nm are strongly adsorbed in SU-8 and mainly expose the surface. Also this could be used in our advantage if the flood exposure is done at deep UV (e.g. by LEDs emitting at ~ 260 nm), because a thinner superficial layer would be exposed. Conditioning of the SU-8 - IPL interface needs further improvement.

Improving the mechanical stability of the stencil and decreasing the divergence of the evaporation beam will further increase the definition of the structures demonstrated in this work. The combination of sacrificial polymer structures with permanent ones opens new possibilities in 3D multi-material MEMS design, also known “4D lithography”. Moreover, this technology opens new possibilities for producing unconventional 3D architectures combining polymeric and metallic structures e.g. for distributed sensing applications.

Acknowledgements

The authors would like to thank Ferruccio Pisanello and Marco Pisanello for their valuable suggestions and helpful discussions during this work.

We would also like to thank Antonio Balena and Alessandro Rizzo for their assistance in thermal evaporation.

References

[1] Paul S.C. Taçon, et al., Ancient bird stencils discovered in Arnhem Land, Northern Territory, Australia, Antiquity 84 (324) (2015) 416–427.
[2] H. Cai, et al., Utilization of resist stencil lithography for multidimensional fabrication on a curved surface, ACS Nano 12 (9) (2018) 9626–9632.
[3] P. Colson, C. Henrist, R. Cloots, Nanosphere lithography: a powerful method for the controlled manufacturing of nanomaterials, J. Nanomater. 2013 (2013) 19.
[4] C.L. Haynes, R.P. Van Duyne, Nanosphere lithography: a versatile nanofabrication tool for studies of size-dependent nanoparticle optics, J. Phys. Chem. B 105 (24) (2001) 5599–5611.
[5] A. Heuberger, X-ray lithography, Microelectronic Engineering, vol. 29, Elsevier, 1986, pp. 93–101 december.
[6] O. Vazquez-Mena, et al., High-resolution resistless nanopatterning on polymer and flexible substrates for plasmonic biosensing using stencil masks, ACS Nano 6 (6) (2012) 5474–5481.
[7] O. Vazquez-Mena, et al., Metallic nanowires by full wafer stencil lithography, Nano Lett. 8 (11) (2008) 3675–3682.
[8] L.G. Villanueva, et al., All-stencil transistor fabrication on 3D silicon substrates, J. Micromech. Microeng. 22 (9) (2012) 095022.
[9] G.J. Dolan, Offset masks for lift-off photoprocessing, Appl. Phys. Lett. 31 (5) (1977) 337–339.
[10] M. Hatzakis, Electron resists for microcircuit and mask production, J. Electrochem. Soc. 116 (7) (1969) 1033–1037.
[11] Henry I. Smith, F.J. Bachner, N. Efremow, A high-yield photolithographic technique for surface wave devices, J. Electrochem. Soc. 118 (5) (1971) 821–825.
[12] O. Vazquez-Mena, et al., Resistless nanofabrication by stencil lithography: a review, Microelectron. Eng. 132 (2015) 236–254.
[13] K. Du, et al., Stencil lithography for scalable micro- and nanomanufacturing, Micromachines 8 (4) (2017) 131.
[14] L.R. Meza, et al., Resilient 3D hierarchical architected metamaterials, Proc. Natl. Acad. Sci. 112 (37) (2015) 11502.
[15] C.M. Soukoulis, M. Wegener, Past achievements and future challenges in the development of three-dimensional photonic metamaterials, Nat. Photonics 5 (2011) 523.
[16] S. Kawata, et al., Finer features for functional microdevices, Nature 412 (2001) 697.
[17] E.D. Lemma, et al., Confocal imaging characterization of two-photon lithography microstructures for cell cultures, 2017 IEEE 17th International Conference on Nanotechnology (IEEE-NANO), 2017.
[18] F. Klein, et al., Elastic fully three-dimensional microstructure scaffolds for cell force measurements, Adv. Mater. 22 (8) (2010) 868–871.
[19] S. Rekštytė, et al., Direct laser fabrication of composite material 3D microstructured scaffolds, JLMN-J. Laser Micro/Nanoeng. 9 (1) (2014) 25–30.
[20] F. Formanek, et al., Three-dimensional fabrication of metallic nanostructures over large areas by two-photon polymerization, Opt. Express 14 (2) (2006) 800–809.
[21] D. Jang, et al., Fabrication and deformation of three-dimensional hollow ceramic nanostructures, Nat. Mater. 12 (2013) 893.
[22] M. Hermatschweiler, et al., Fabrication of silicon inverse woodpile photonic crystals, Adv. Funct. Mater. 17 (14) (2007) 2273–2277.
[23] J.K. Gansel, et al., Gold helix photonic metamaterial as broadband circular polarizer, Science 325 (5947) (2009) 1513.
[24] T. Jonavičius, S. Rekštytė, M. Malinauskas, Microfabrication of 3D metallic interconnects via direct laser writing and chemical metallization, Lith. J. Phys. 54 (3) (2014) 162–169.
[25] W. Kristof, P. Robert, Diffusing and swelling in SU-8: insight in material properties and processing, J. Micromech. Microeng. 20 (9) (2010) 095013.